Wind tunnel measurements of indoor air quality in a building with natural cross-ventilation

S. F. Díaz-Calderón

Instituto de Energías Renovables, Universidad Nacional Autónoma de México, Priv. Xochicalco s/n, Col. Centro, 62580 Temixco, Mor., México.

C. Gromke

Laboratory of Building and Environment Aerodynamics, Institute for Water and Environment, Karlsruhe Institute of Technology, Kaiserstrasse 12, 76128, Karlsruhe, Germany.

J. A. Castillo

Facultad de Ingeniería, Universidad Veracruzana, Campus Coatzacoalcos, Av. Universidad Km 7.5, Col. Santa Isabel, 96538 Coatzacoalcos, Ver., Mexico.

G. Huelsz

Instituto de Energías Renovables, Universidad Nacional Autónoma de México, Priv. Xochicalco s/n, Col. Centro, 62580 Temixco, Mor., México, e-mail: ghl@ier.unam.mx

Received 12 June 2024; accepted 16 August 2024

In recent years, there has been an increase in indoor air quality studies in buildings, which examine minimum requirements to reduce the probability of respiratory disease transmission. These studies are primarily conducted in existing buildings, with fewer evaluations of generic geometry buildings in wind tunnels. These experimental studies are valuable, among other things, for validating numerical models of Computational Fluid Dynamics (CFD). This study employs the experimental technique of electron capture detection to obtain the distribution of a tracer gas throughout the interior volume of a scaled building with cross-ventilation in a modelled atmospheric boundary layer flow. The building is considered isolated (without neighbors) and features windows at the same bottom height of the windward and leeward facades. A facade porosity (the ratio of area between the window and the facade) of 10% is considered. Maintaining geometric and dynamic similarity, the results are scaled based on a building height of 2.8 m and an incident wind velocity at the building height of 0.85 m/s. Under these conditions, the values of air exchange rate $I = 0.0167$ s^{-1}, nominal time $\tau_n = 60$ s, and 60 air changes per hour (ACH) are calculated. It is anticipated that the concentration results presented in this study will be utilized in future validations of CFD models.

Keywords: Natural ventilation; indoor air quality; wind tunnel measurements; tracer gas; electron capture detection.

DOI: https://doi.org/10.31349/RevMexFis.71.010601

1. Introduction

In the recent context of the COVID-19 pandemic, due to the spread of the SARS-CoV-2 [1], experimental studies on indoor air quality (IAQ) in buildings have increased. The transmission of respiratory diseases is attributed to three factors: contact with infected surfaces, short-term droplet transmission, and long-term airborne transmission [2]. The latter is the primary focus of ventilation studies in buildings, aiming to determine the minimum indoor air renovations to reduce the probability of transmission [2].

For educational buildings, a minimum of six air changes per hour ACH [1/h] has been established, as recommended by Harvard University School of Public Health [4] and the Lancet COVID-19 Commission [5]. In Mexico, the construction regulations of Mexico City [6] also recommend the same value without distinguishing between the use of natural or mechanical ventilation. The risk of SARS-CoV-2 infection, estimated using the Wells-Riley model, is less than 1% when a face mask is used and $6.5 \leq ACH$. Without a face mask, the risk remains below 1% only for $22.0 \leq ACH$ [7].

Natural ventilation (NV) is a bioclimatic design strategy used to achieve hygrothermal comfort in warm climates or seasons [8,9]. NV is also recommended for achieving healthy values of IAQ by removing carbon dioxide, bad odors, and infectious particles [10,11]. NV is generated by the pressure difference between openings (windows and doors) on the building facades [12,13]. Wind-driven NV, resulting from wind incidence, is studied using a scale model of the building in a wind-tunnel [14]. In the latter study, the building is considered isolated (without neighboring buildings), with windows located on two different facades (adjacent or opposite). The size and location of the windows are varied and the indoor velocity distribution in different planes is obtained. This experimental study is used for validating Computational Fluid Dynamics (CFD) numerical models [15-17]. Recent IAQ studies utilizing CFD simulations, where the in-

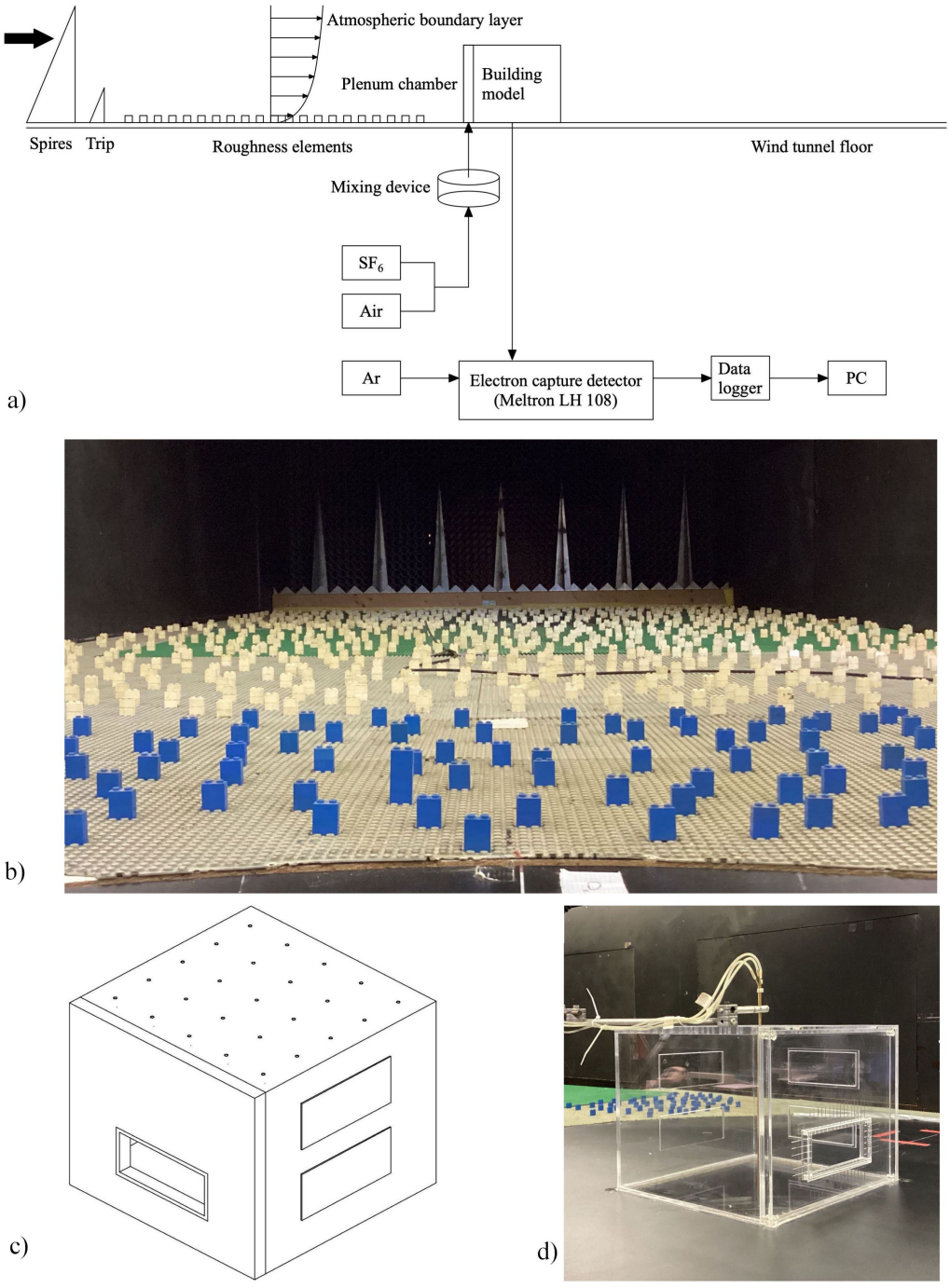

FIGURE 1. Experimental set-up: a) scheme of the wind-tunnel, the tracer gas injection, and the concentration measurements; based on [22]; b) view of spires, trips and roughness elements in the wind-tunnel; c) scheme of the building model with different cross-ventilation configurations; d) view of the building model in the wind-tunnel.

door air renovation is calculated, are validated using experimental data of velocity [18,19] and pressure [20].

Two NV studies have focused on obtaining the indoor distribution of a tracer gas in buildings with cross-ventilation in wind tunnels. Both studies test windows on opposite facades, with the tracer gas source located at the floor of the building. The first study [21] considers a geometry similar to that of [14], with windows at the center of the windward and the leeward facades, and the source of the tracer gas is a point at the center of the floor. The authors report the distribution of the tracer gas in the vertical streamwise central plane. The second study [22] considers a cubic geometry with vertical and elongated windows at the center of the lateral facades. This study employs a homogeneous source of the tracer gas across the entire floor. The indoor distribution of the tracer gas in the entire indoor air volume is measured

and the value of ACH is reported. Both studies could be utilized for the validation of CFD simulations considering the same input conditions of the experiment.

The present wind tunnel measurements apply the methodology reported by [22] to obtain the tracer gas distribution in the entire indoor air volume of a building with cross-ventilation. The ACH calculation is also provided. The building geometry from [14] is adopted. The building is isolated, and the wind is perpendicular to the windward facade. The windows are located at the bottom height of the windward and leeward facades. The tracer gas injection occurs within the frame of the windward window (Fig. 1). The experimental methodology is detailed in Sec. 2, the evaluation parameters are provided in Sec. 3, the results and the analysis are presented in Sec. 4, and in Sec. 5, the conclusions and future work are outlined.

2. Experimental methodology

2.1. Wind-tunnel

The measurements are conducted in an atmospheric boundary layer wind tunnel in the Laboratory of Building and Environmental Aerodynamics at the Karlsruhe Institute of Technology (KIT) [Fig. 1a)]. The wind tunnel has a test section of 2×1 m^2 (width $\times$ height). The ceiling of the wind tunnel can be adjusted to achieve a zero gradient of the pressure in the streamwise direction ($\delta p/\delta x = 0$). To generate an atmospheric boundary layer in the test section, a series of flow straighteners (honeycomb), Irwin-type vortex generators (spires and trip), a horizontally ground-mounted tripping device, and 6 m of fetch covered with roughness elements of 2 cm of height are used [Fig. 1b)]. The atmospheric boundary layer was characterized, mean velocity $u(y)$ [m/s] and turbulence intensity $I(y)$ [-] profiles were reported [22]. The present work uses this characterization to estimate $u(y)$, considering a different building height y_{ref} and free stream velocity u_∞. The function $u(y)$ is estimated using:

$$u(y) = u_{\text{ref}} \left(\frac{y-d}{y_{\text{ref}}} \right)^{\alpha}, \tag{1}$$

where u_{ref} is the reference velocity, $d = 0$ is the displacement thickness, and $\alpha = 0.28$ is the power law exponent (urban region). The value of $u_\infty = 10.00$ m/s is measured at the boundary layer height $\delta = 0.5$ m. Therefore, at $y_{\text{ref}} = 0.28$ m the value $u_{\text{ref}} = 8.51$ m/s is calculated. Figure 2 shows the experimental profiles of $u(y)$ and $I(y)$ taken from [22].

The reference time t_{ref} is calculated using:

$$t_{\text{ref}} = \frac{y_{\text{ref}}}{u_{\text{ref}}}, \tag{2}$$

therefore $t_{\text{ref}} = 0.033$ s.

The building Reynolds number Re_b [-] is calculated using:

$$Re_b = \frac{u_{\text{ref}} y_{\text{ref}}}{\nu}, \tag{3}$$

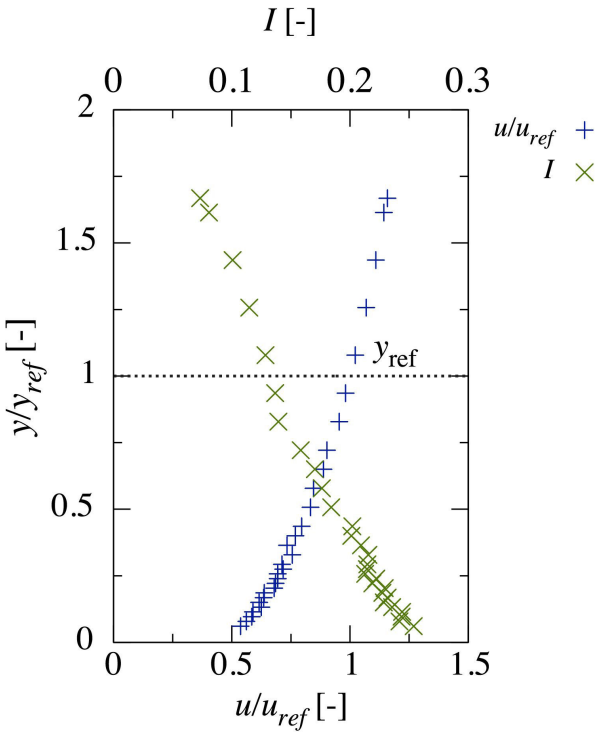

FIGURE 2. Experimental profiles of normalized velocity u/u_{ref} and turbulence intensity I. Taken from [22].

where $\nu = 1.57 \times 10^{-5}$ m^2/s is the kinematic viscosity of the air. A value of $Re_b = 1.52 \times 10^5$ is calculated, ensuring independence with regards to Re_b [23].

2.2. Model of the building

A building model with cross-ventilation and various configurations of the windows is designed for wind tunnel measurements of IAQ. The model is manufactured using transparent acrylic. Figure 1c) shows a sketch of the model, and Fig. 1d) shows an image of the model in the wind tunnel. The external dimensions of the model are $0.35 \times 0.35 \times 0.28$ m^3 (width $\times$ length $\times$ height). A facade porosity P [-] (ratio of window to facade area) of 0.10 is considered. Thus, the dimensions of the windows are 0.161×0.063 m^2 (width $\times$ height). The window on the windward facade is fixed at a bottom position, at a height of $y = 0.0525$ m (lower edge of the window). On the leeward and right-adjacent facades, windows can be opened or closed at both bottom and top positions, the latter at a height of $y = 0.1645$ m (lower edge of the window), using caps, allowing for different cross-ventilation configurations using the same building model. In this work, the bottom window on the leeward facade is considered. The model represents a building at full scale. The experiments maintain geometric and dynamic similarity with the full scale. The scale factor between the full-scale building and the model is 10:1. The reference velocity at full scale is determined by maintaining the same Reynolds number, Re_b.

A plenum chamber is used for tracer gas injection in front of the building model (windward facade). The chamber has

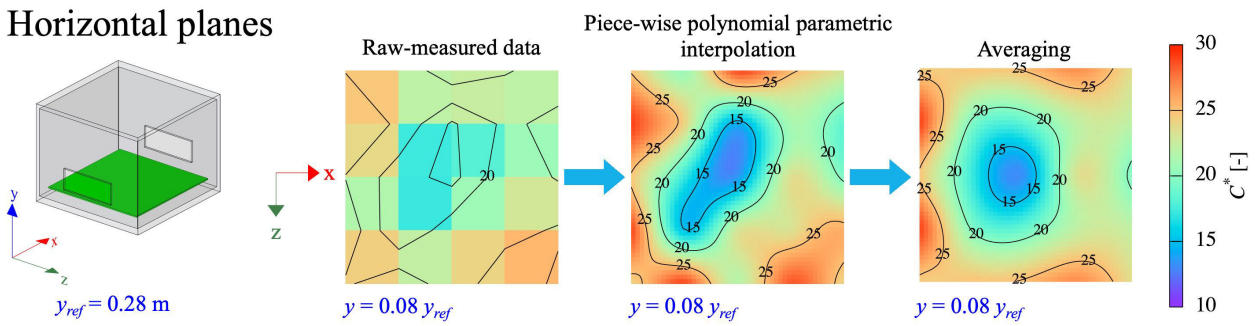

FIGURE 3. Methodology to obtain contour plots of C^*: raw-measured data, piece-wise polynomial parametric interpolation, and averaging in symmetric points. Example for a horizontal plane.

a thickness of 0.0210 m, which is included in the external length of the building model. A mixture of pressured air (carrier gas) and sulfur hexafluoride (SF_6, tracer gas), is injected into the airflow in the window frame using a set of 44 needles [Fig. 1d)]. The needles have a length of 0.0400 m and an inner diameter of 0.0006 m, with a distance of 0.0050 m between them.

The roof of the model building has 25 equidistant holes (0.0650 m apart), distributed in five lines of five holes from right to left [Fig. 1c)]. These sealable holes are used to insert a probe for the concentration measurements [Fig. 1d)]. Each hole has a diameter of 0.0045 m.

2.3. Tracer gas concentration measurements

The tracer gas constant injection method is employed [24]. The indoor distribution of the concentration in a steady state is obtained using the experimental technique of electron capture detection (ECD) (model: Meltron LH 108) [Fig. 1a)]. A mixture of pressured air and SF_6 with mass flows of 700 and 24 cm^3/min, respectively, is controlled using MKS Flowrate Controllers. A mixing device is used to achieve good mixing of the gases before the filling of the plenum chamber. The mixture is injected into the inflow jet in the frame of the windward window using equidistant needles. The concentration in the indoor of the building model is sampled using an external probe inserted through the roof [Fig. 1d)]. The probe has three sample taps with a distance of 0.0440 m between them. For each hole in the roof, the probe is positioned at two different heights to obtain six measurements. A total of 150 points are considered to obtain the indoor distribution of concentration in the entire indoor air volume V [m^3].

3. Evaluation parameters

The experimental results of concentration are provided in their normalized form:

$$C^* = \frac{u_{ref} y_{ref} C}{S/l}, \tag{4}$$

where C [cm^3/m^3] is the local concentration, S [cm^3/s] is the volumetric flow rate of the tracer gas along the perimeter of the window, and l [m] is the length of the perimeter. The air exchange rate I [1/s] is calculated as follows [22]:

$$I = \frac{S}{\overline{C} V}, \tag{5}$$

where $\overline{C}$ is the average of the concentration in V. The nominal time τ_n is calculated considering the inverse value of I [24]. The air changes per hour ACH [1/h] are calculated according to:

$$ACH = \frac{3600}{\tau_n}. \tag{6}$$

4. Results and analysis

Contour plots of C^* are employed to analyze indoor distribution. The software Gnuplot 5.5 [25] is utilized for representing the results. Figure 3 illustrates the methodology followed to obtain the contour plots of C^*, using as an example a horizontal plane. In the contour plot of raw-measured data, the vertices of each square represent the measured data. The color of the square corresponds to the average of the four vertices. To smooth the isolines, interpolation using the piece-wise polynomial parametric method is applied. Both the averaging of the vertex values and the refinement by the interpolation increase (or decrease) the C^* values at the contour limits. The maximum difference between the measured and the interpolated data, considering the average of C^* of all points in V, is up to 5%. Averaging at symmetric points is applied. The maximum difference between the measured and the averaged data is up to 15%. However, interpolation and averaging are solely considered for visualization. The evaluation of NV and IAQ using the evaluation parameters is based on the raw-measured data. The interpolation and averaging in symmetric cases are previously reported in comparable studies of concentration measurements [22,26].

4.1. Concentration indoor distribution

To analyze the indoor distribution of C^*, vertical planes that are normal or parallel to the direction of the wind, as well as horizontal planes (Fig. 4), are utilized. Three vertical normal planes to the wind are considered. These are planes

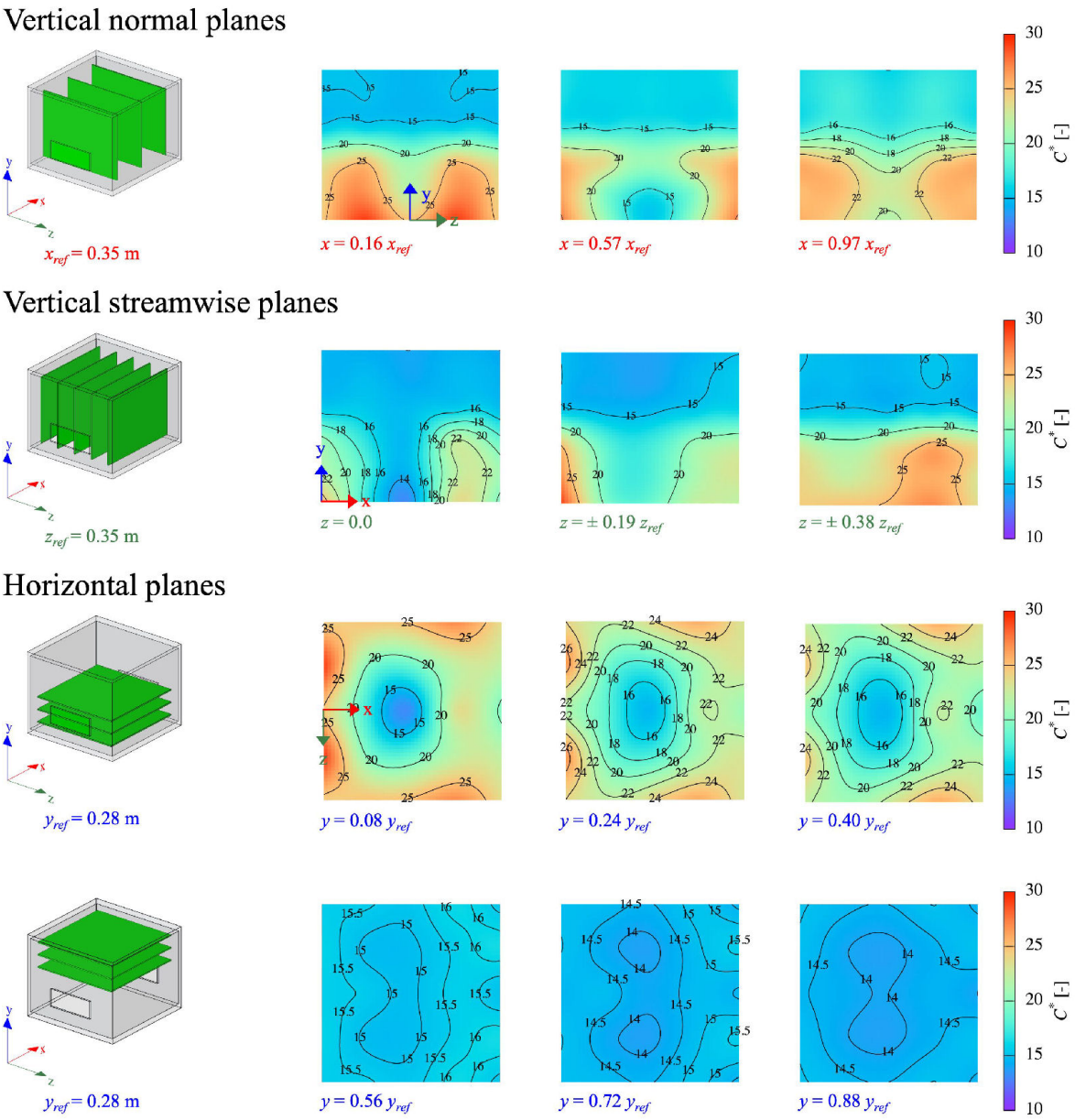

FIGURE 4. Normalized concentration C^* results.

at $x = 0.16x_{\text{ref}}$ (close to the windward facade), $x = 0.57x_{\text{ref}}$ (close to the center), and $x = 0.97x_{\text{ref}}$ (close to the leeward facade), where $x_{\text{ref}} = 0.35$ m. Five vertical streamwise planes are analyzed. Given the configuration of windows, these planes are symmetric around the central plane ($z = 0.0$). Therefore, besides the central plane, two more are reported for $\pm 0.19 z_{\text{ref}}$ and $\pm 0.38 z_{\text{ref}}$, where $z_{\text{ref}} = 0.35$ m. Six horizontal planes are reported. The first one is located at $y = 0.08 y_{ref}$, where $y_{ref} = 0.28$ m. The distance between consecutive planes is $0.16 y_{\text{ref}}$.

Figure 4 illustrates the indoor distribution of C^*. In general, the highest values of C^* are located in the bottom zone. The first vertical normal plane ($x = 0.16x_{\text{ref}}$) exhibits an increase of C^* near the lateral sides of the window, reaching up to $C^* = 25.0$. In contrast, the values decrease to as low as $C^* = 20.0$ near the center of the window. This indicates that the injection of the tracer gas is not homogeneous across the window area. It can be observed that the highest values of C^* (20.0 to 30.0) are found in the bottom half part of the building indoors and around the vertical central axis. At the center region of the bottom half part, C^* decreases to 15.0. The upper half part of the building has C^* values in the range of 14.5 to 15.5. As can be seen in [14], for this configuration of windows, the bottom part of the building is characterized by high air velocity magnitude as the jet flow crosses it. Thus, the distribution of C^* within the building indoors is due to the non-homogeneity of the tracer gas injection in the windward window in combination with high flow velocities at the bottom part of the building.

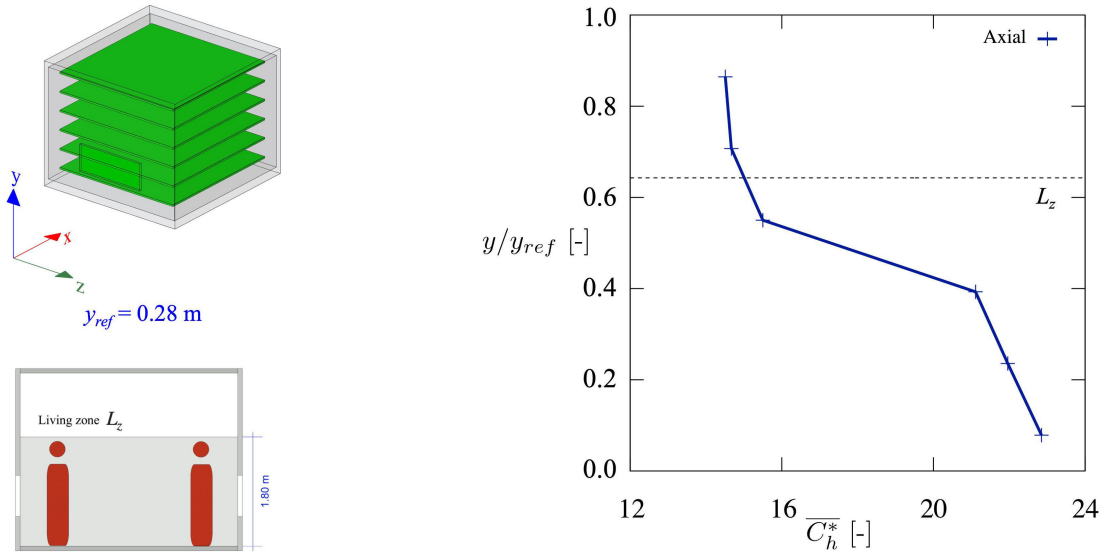

FIGURE 5. Average of C^* in the horizontal planes ($\overline{C_h^*}$). The horizontal planes and the living zone (height up to 1.8 m) are shown.

Figure 5 depicts the variation of the average of C^* in the horizontal planes, denoted by $\overline{C_h^*}$, as a function of height. In the living zone L_z, up to a height of 1.8 m, the maximum value of $\overline{C_h^*}$ is found on the plane closest to the floor $y = 0.08y_{\text{ref}}$, reaching $\overline{C_h^*} = 22.9$. $\overline{C_h^*}$ decreases with increasing height. The most significant reduction occurs between the heights of $y = 0.40y_{\text{ref}}$ and $0.56y_{\text{ref}}$, where $\overline{C_h^*}$ decreases from 21.1 to 15.5, a reduction of 27%. Considering the maximum value of $\overline{C_h^*}$, the reduction with respect to the highest level in L_z ($y = 0.56y_{\text{ref}}$) is 32%.

4.2. Air renovation evaluation

The calculation of the air renovation is conducted at a real scale. The nominal time (τ_n) is scaled using the relation between reference times:

$$\frac{\tau_{n,ls}}{t_{\text{ref},ls}} = \frac{\tau_{n,rs}}{t_{\text{ref},rs}}, \tag{7}$$

where the subscripts $_{ls}$ and $_{rs}$ denote laboratory and real scales, respectively. In the laboratory scale, the values of $y_{\text{ref},ls} = 0.28$ m, $u_{\text{ref},ls} = 8.51$ m/s, and $t_{\text{ref},ls} = 0.033$ s, $S = 24$ cm^3/min, $V = 0.0279$ m^3, and $\overline{C} = 8.59$ cm^3/m^3 are utilized. Correspondingly, in the real scale, the values become $y_{\text{ref},rs} = 2.80$ m, $u_{\text{ref},rs} = 0.85$ m/s, and $t_{\text{ref},rs} = 3.30$ s. The results of $I = 0.0167$ s^{-1}, $\tau_n = 60$ s, and 60 ACH are obtained. The minimum requirement specified by the construction regulation of Mexico City [6] for educational buildings (6 ACH) is achieved.

5. Conclusions and future work

This article presented wind tunnel measurements of the distribution of a tracer gas throughout the interior of a building with cross-ventilation. An isolated building (without neighbors) with windows located at the lower height of the windward and leeward facades was considered. The facade porosity was set at 10%. The tracer gas injection was carried out at the window frame on the windward facade, and the electron capture detector technique was used to measure the concentration at 150 points throughout the indoor air volume of the building.

The highest concentrations were observed in the areas closest to the lateral sides of the window on the windward facade, along with a decrease in concentration in the area near the center of the window, indicating non-uniform tracer gas injection. It was observed that the highest concentrations were located in the lower zone of the building, with a decrease in concentration as the height increased. Within the living zone, a reduction of up to 32% in concentration was achieved as the height increased.

The calculation of air renovation parameters for the real scale results in an air exchange rate of $I = 0.0167$ s^{-1}, nominal time $\tau_n = 60$ s, and air changes per hour $ACH = 60$. This last value far exceeds the minimum requirements for healthy ventilation.

In future work, it is recommended that the tracer gas injection be refined, aiming for a more homogeneous gas entry into the window. It is suggested that the effect of varying the cross-ventilation configuration be investigated and the impact of facade porosity on the interior concentration distribution be explored. Additionally, future work should consider analyzing the effect of wind incidence angle, the urban environment, and the inclusion of indoor obstacles on the ACH value. Furthermore, it is anticipated that the concentration results obtained in this study will be utilized in future validations of Computational Fluid Dynamics numerical models.

Acknowledgments

The authors extend their gratitude to Armin Reinsch, Juergen Ulrich, and Michael Ziegler for their technical support during the wind tunnel experiments. This study was partially supported by PAPIIT-UNAM IT101824 project. S. F. Díaz-Calderón acknowledges the doctoral scholarships granted by the General Coordination of Graduate Studies UNAM and by CONAHCyT, with numbers 518004712 and 795223, respectively.

1. L. Wang *et al.*, Review of the 2019 novel coronavirus (SARSCoV- 2) based on current evidence, *International Journal of Antimicrobial Agents* **55** (2020) 105948, https://doi.org/10.1016/j.ijantimicag.2020.105948.
2. J. S. Kutter *et al*., Transmission routes of respiratory viruses among humans, *Current Opinion in Virology* **28** (2018) 142, https://doi.org/10.1016/j.coviro.2018.01.001.
3. D. Lewis, Indoor Air is full of flu and COVID viruses. will countries clean it up?, https://www.nature.com/articles/d41586-023-00642-9 (2023), Last checked March, 2023.
4. J. E. *et al.*, SCHOOLS FOR HEALTH: Risk Reduction Strategies for Reopening Schools. Harvard T.H. Chan School of Public Health Healthy Buildings program, https://schools.forhealth.org/wp-content/uploads/sites/19/2020/06/Harvard-Healthy-Buildings-Program-Schools-For-Health-Reopening-pdf. (2020), Last checked May, 2023.
5. The Lancet COVID-19 Commission Task Force on Safe Work, Safe School, and Safe Travel, Proposed Non-infectious Air Delivery Rates (NADR) for Reducing Exposure to Airborne Respiratory Infectious Diseases, https://covid19commission.org/commpub/lancet-covid-commission-tf-report-nov-2022+. (2022), Last checked May, 2023.
6. Gobierno de México, Norma Técnica Complementaria Para El Proyecto Arquitectónico, https://cgservicios.df.gob.mx/prontuario/ vigente/r406001.pdf (2011), Last checked May, 2023.
7. S. Park *et al.*, Natural ventilation strategy and related issues to prevent coronavirus disease 2019 (COVID-19) airborne transmission in a school building, *Science of The Total Environment* **789** (2021) 147764, https://doi.org/10.1016/j.scitotenv.2021.147764.
8. W. Liping and W. N. Hien, The impacts of ventilation strategies and facade on indoor thermal environment for naturally ventilated residential buildings in Singapore, *Building and Environment* **42** (2007) 4006, https://doi.org/10.1016/j.buildenv.2006.06.027.
9. J. Park and G. H. Rhee, Comparison of volume flow rate and volume-averaged local mean age of air for evaluating ventilation performance in natural ventilation, *Journal of Mechanical Science and Technology* **31** (2017) 5801, https://doi.org/10.1007/s12206-017-1122-0.
10. A. Aflaki *et al.*, A review on natural ventilation applications through building façade components and ventilation openings in tropical climates, *Energy and Buildings* **101** (2015) 153, https://doi.org/10.1016/j.enbuild.2015.04.033.
11. R. K. Bhagat, *et al*., Effects of ventilation on the indoor spread of COVID-19, *Journal of Fluid Mechanics* **903** (2020) F1, https://doi.org/10.1017/jfm.2020.720.
12. D. Etheridge, A perspective on fifty years of natural ventilation research, *Building and Environment* **91** (2015) 51 , https://doi.org/10.1016/j.buildenv.2015.02.033.
13. B. Blocken, Computational Fluid Dynamics for urban physics: Importance, scales, possibilities, limitations and ten tips and tricks towards accurate and reliable simulations, *Building and Environment* **91** (2015) 219, https://doi.org/10.1016/j.buildenv.2015.02.015.
14. P. Karava, T. Stathopoulos, and A. Athienitis, Airflow assessment in cross-ventilated buildings with operable faÃ§ade elements, *Building and Environment* **46** (2011) 266, https://doi.org/10.1016/j.buildenv.2010.07.022.
15. R. Ramponi and B. Blocken, CFD simulation of crossventilation for a generic isolated building: Impact of computational parameters, *Building and Environment* **53** (2012) 34, https://doi.org/10.1016/j.buildenv.2012.01.004.
16. J. Perén *et al*., CFD analysis of cross-ventilation of a generic isolated building with asymmetric opening positions: Impact of roof angle and opening location, *Building and Environment* **85** (2015) 263, https://doi.org/10.1016/j.buildenv.2014.12.007.
17. S. Díaz-Calderón, J. Castillo, and G. Huelsz, Evaluation of different window heights and facade porosities in naturally cross-ventilated buildings: CFD validation, *Journal of Wind Engineering and Industrial Aerodynamics* **232** (2023) 105263, https://doi.org/10.1016/j.jweia.2022.105263.
18. K. Kosutova *et al.*, Cross-ventilation in a generic isolated building equipped with louvers: Wind-tunnel experiments and CFD simulations, *Building and Environment* **154** (2019) 263, https://doi.org/10.1016/j.buildenv.2019.03.019.
19. S. Díaz-Calderón, J. Castillo, and G. Huelsz, Indoor air quality evaluation in naturally cross-ventilated buildings for education using age of air, *Journal of Physics: Conference Series* **2069** (2021) 012182, https://doi.org/10.1088/1742-6596/2069/1/012182.
20. H. Montazeri and F. Montazeri, CFD simulation of crossventilation in buildings using rooftop wind-catchers: Impact of outlet openings, *Renewable Energy* **118** (2018) 502, https://doi.org/10.1016/j.renene.2017.11.032.

21. Y. Tominaga and B. Blocken, Wind tunnel experiments on cross-ventilation flow of a generic building with contaminant dispersion in unsheltered and sheltered conditions, *Building and Environment* **92** (2015) 452, https://doi.org/10.1016/j.buildenv.2015.05.026.

22. V. Pappa *et al*., A wind tunnel study of aerodynamic effects of façade and roof greening on air exchange from a cubic building, *Building and Environment* **231** (2023) 110023, https://doi.org/10.1016/j.buildenv.2023.110023.

23. I. P. Castro and A. G. Robins, The flow around a surface-mounted cube in uniform and turbulent streams, *Journal of Fluid Mechanics* **79** (1977) 307, https://doi.org/10.1017/S0022112077000172.

24. ISO, ISO 16000-8:2007(en), Indoor air-Part 8: Determination of local mean ages of air in buildings for characterizing ventilation conditions (2007).

25. T. Williams and C. Kelley, Gnuplot 5.5: An interactive plotting program (Version 5.5 organized by: Ethan A Merritt and many others), https://www.gnuplot.info/docs_5.5/gnuplot.pdf (2021), Last checked February, 2024.

26. C. Gromke and B. Ruck, On the Impact of Trees on Dispersion Processes of Traffic Emissions in Street Canyons, *Boundary-Layer Meteorology* **131** (2009) 19, https://doi.org/10.1007/s10546-008-9301-2.